Received: 21 July 2023 | Revised: 19 December 2023 | Accepted: 26 January 2024

DOI: 10.1002/we.2901

RESEARCH ARTICLE

WILEY

On the use of secondary rotors for vertical axis wind turbine power take-off

Laurence Morgan | William Leithead | James Carroll

EEE, University of Strathclyde, Glasgow, UK

Correspondence
Laurence Morgan, EEE, University of Strathclyde, Glasgow, G1 1XW, UK.
Email: laurence.morgan@strath.ac.uk

Funding information
XROTOR, EU H2020, Grant/Award Number: 101007135; Centre for Doctoral Training in Wind and Marine Energy Systems, EPSRC, Grant/Award Number: EP/S023801/1.

Abstract

This work introduces and explores the use of secondary rotors for vertical axis wind turbine power take-off. A parametric framework based on optimally designed secondary rotors is developed which calculates the maximum achievable efficiency of power conversion between the primary and secondary rotors. It is shown that practicable rotor designs can convert between 87% and 90% of primary rotor power to the secondary rotors whilst facilitating nacelle mass reductions between 85% and 87% compared to traditional reference turbine drivetrains.

KEYWORDS
drivetrain, power take-off, secondary rotor, VAWT, X-Rotor

1 | INTRODUCTION

Part one of the Intergovernmental Panel on Climate Change's AR6 report states that rapid and large-scale reductions to greenhouse gas emissions must be enacted this decade in order to limit global warming to close to 1.5°C or even 2°C, averting the most catastrophic effects of the climate crisis.[1] The pathway to a 1.5° future is contingent on significant increases in renewable-generated electricity.[2] This transition must be led by the rapid deployment of wind energy, with the annual installed capacity of wind energy required to more than triple between 2021 and 2030.[3] Reducing the cost of energy for offshore wind is key to increasing the rate at which offshore wind capacity is deployed, this is especially pertinent for floating offshore wind where costs are still are a barrier to commercialization. Decreasing the cost of energy can typically be achieved through either incremental innovation or radical innovation; this work focuses on the latter, exploring the use of secondary rotors to provide wind turbine power take-off. It has previously been shown that the use of secondary rotors in conjunction with a vertical axis wind turbine (VAWT) has the potential to reduce the cost of offshore wind energy by up to 26%.[4] This work does not seek to provide cost of energy analysis but will attempt to characterize and investigate the interaction between primary and secondary rotors to inform the coupled design of turbines that utilize secondary rotors for power take-off optimized to maximize energy capture.

Traditionally wind turbine power take-off is completed through an electrical machine connected to the rotor shaft either directly or through a gearbox as a sub-system referred to as the drivetrain.[5] Due to the low rotational speed of the wind turbine rotor, the input torque is typically very high leading to heavy, expensive drivetrains. Additionally, as these drivetrains are located at the rotor hub height (typically in excess of 100 m above sea level), the operations and maintenance costs associated with the drivetrain are also large due to the cost of scheduling heavy lift vessels for large component repairs. In general, a wind turbine's nacelle accounts for approximately 50% of turbine capital costs,[6] and maintenance associated with the drivetrain accounts for between 49% and 59% of the wind turbine downtime (based on drivetrain configuration)[7] and 69% of the

Abbreviations: BEM, blade element momentum theory; EESG, electrically excited synchronous generator; HAWT, horizontal axis wind turbine; LLFVW, lifting line free vortex wake; PMSG, permanent magnet synchronous generator; VAWT, vertical axis wind turbine.

William Leithead and James Carroll contributed equally.

material cost of repairs, as calculated combining failure rate data and material cost data from.[8] This indicates that innovation in wind turbine power take-off has the potential to significantly decrease the cost of energy, both in terms of capital and operational expenditure.

In order to increase the conversion efficiency and the drivetrain reliability, large offshore wind turbines are converging on the use of permanent magnet synchronous generators (PMSGs),[9] either in a direct drive configuration or utilizing a medium-speed gearbox. The production of these PMSGs requires the extraction of rare earth metals including neodymium, praseodymium, dysprosium and terbium.[10] Humanitarian issues have been raised around the methods of extraction, and the geographic distribution of the mineral deposits (with the majority based in China) has led to concerns around geopolitical disruptions to the supply chain.[11] Finally, the limited size of these mineral deposits and the projected scale of global demand have been shown to potentially cause a bottleneck for offshore wind energy deployment,[12] although the scale of this issue is contended.[13] Whilst, for reliability reasons, PMSGs are likely to be employed in secondary rotor systems, the torque reduction facilitated by the use of a secondary rotor significantly decreases the volume of material required, mitigating these issues. Electrically excited synchronous generators (EESGs) have been identified as a solution for rare-earth-free wind turbine generators; however, their excessive mass, lower efficiency and the requirement for slip rings (and the associated reliability issues) are currently barriers to adoption in the offshore environment. In the case of VAWTs, as the drivetrain can be located at sea level, the issues around the generator mass are not as pertinent and EESGs are therefore a more viable option. The additional maintenance actions associated with the slip ring, the lower power conversion efficiency and the increased cost associated with the large mass still represent problems that can be overcome by the use of secondary rotors.

In addition to the current costs associated with wind turbine drivetrains, the traditional drivetrain concept also has issues with up-scaling. The power available to wind turbines scales with the swept area $\left(l^2\right)$; however, as the rotor tip speed is limited, the rotor speed scales inversely to the radius increase $\left(l^1\right)$; thus, the rotor torque, and therefore generator volume, scales with the cube of the length scale $\left(l^3\right)$. This square-cube relationship between the revenue (power captured) and costs (proportional to the mass/volume of components) is often highlighted when considering the costs of the rotor structure[14]; however, here, it is referring directly to the generator costs when upscaled subject to a tip-speed limit. Despite this square-cube law, rotor up-scaling has thus far remained attractive as it can offer significant savings to the balance of plant and operations and maintenance costs. Whilst it has been shown that real up-scaling has thus far 'beaten' the square-cube law,[14] likely due to technological development occurring parallel to upscaling, wind turbine designs that circumvent these scaling laws altogether should be considered to facilitate economically viable up-scaling in the future. The recent increase in research work on multi-rotor systems[15] indicates that the wind energy community is taking seriously the prospect of radical innovation to facilitate the further up-scaling of wind turbine systems. Secondary rotors provide a means of increasing the power take-off capacity that scales linearly with the power captured, as additional secondary rotor systems can added rather than up-scaling the individual drivetrain and can therefore provide a solution to the up-scaling problem.

Whilst tip rotors had previously been studied in the context of helicopter flight from the start of the 1950s,[16] the first reference on the use of secondary rotors for wind turbine power take-off identified by the authors was found in.[17] The use of 'tip turbines' is dismissed out of hand as the issues concerning blade loading and the gyroscopic effects on the turbine are considered more complex than the gearing issue associated with the low-speed drivetrain. It should be noted that this judgement was made when the typical wind turbine had a rated power of 30 kW and a rotor diameter of 10 m.[18] The re-evaluation of this technology, given the size and scale of the next generation of wind turbines (>240 m rotor diameter and >15 MW power rating), is therefore deemed understandable. In Watson et al,[15] a survey of emerging technologies in the wind energy sector included a discussion on the use of secondary rotors attached to the rotor blade tips, including a brief discussion on the potential power density of the generators. A thorough discussion of the concept was however outside of the scope of the review paper. In Jamieson,[19] the design of secondary rotors was expanded on further. Specifically, the use of an actuator disk representation including tip losses allowed the author to examine the effects of the design induction factor on the efficiency of energy conversion. In this work the secondary rotor radius was taken as a free design variable and the constraints on secondary rotor design were not explicitly imposed. The use of twin secondary rotors was also discussed, noting that the low induction factor increases the potential for energy capture.

The use of secondary rotors on VAWTs is introduced in Leithead et al[4] as the X-Rotor concept. The article focuses on the presentation of key results of a feasibility study, including the definition of an exemplar 5 MW turbine design and the estimated cost of energy savings achieved by the X-Rotor system. It highlights the design synergies between using a vertical axis wind turbine with secondary rotors, and details cost of energy calculations which demonstrate the potential benefits from secondary rotors (savings of up to 26% on the cost of energy). Due to its broad scope, the discussions on the use of secondary rotors are limited, and the process by which secondary rotors are designed is not discussed. Following the feasibility study which culminated in the publication of Leithead et al,[4] the X-Rotor project successfully obtained H2020 grant funding to continue researching the concept.[20,21] A non-technical rendering of the turbine concept is shown in Figure 1.

McMorland[22] examined areas of O&M cost modelling of novel offshore wind turbine concepts including the X-Rotor. Flannigan[23] presented a modified O&M cost model that facilitates the modelling of X-Rotor systems. The O&M costs for an X-Rotor turbine were compared with conventional horizontal axis wind turbines (HAWTs) of equal power rating, and it is found that the X-Rotor could introduce savings between 20% and 40% compared to a conventional HAWTs (based on drivetrain configuration). Morgan[24] presented the development and validation of a double multiple streamtube model to model the X-Rotor primary rotor, which demonstrated that the primary rotor could achieve power coefficients up to 0.45, more than 10% larger than the value considered in the feasibility study.[4]

FIGURE 1 A non-technical rendering of the X-Rotor concept, showing the X-shaped primary rotors and the secondary rotors attached to the lower blade tips.

This work expands past the existing literature on secondary rotors, introducing a holistic approach to the design of a VAWT that utilizes secondary rotors. Firstly, the requirements for secondary rotors are understood through the derivation of the secondary rotor thrust coefficient required for optimal torque control of the primary rotor, and the efficiency of energy conversion between the primary and secondary rotors in Section 2.1. Limitations on the design of the secondary rotors, arising from both drivetrain constraints and aerodynamic considerations, are then discussed in Section 2.2. In Section 2.3, blade element momentum (BEM)–based optimal design theory is expanded to include high blockage scenarios, and the process of designing the optimal rotor for an arbitrary design thrust coefficient and tip speed ratio is described. Power and thrust coefficient estimates generated by BEM-based optimal design theory are validated first against steady BEM simulations in Section 2.3 and then against lifting line free vortex wake (LLFVW) simulations representative of the aerodynamic environment of the secondary rotors in Section 2.4. The assumptions around the inflow speed for primary rotors are validated using LLFVW simulations of an exemplar primary rotor in Section 2.4.

The ability to accurately obtain on-design aerodynamic coefficients for optimally designed rotors with an arbitrary thrust coefficient and tip speed ratio is then used to generate a parametric framework in Section 3, which facilitates the exploration of the design space of coupled primary–secondary rotor systems. Results from this framework are presented in Section 4, and insights are then drawn in terms of optimal primary rotor design/operation, scalability of turbines utilizing secondary rotors and the effects of various design variables on the efficiency of power conversion between the primary and secondary rotors in Section 5. Final conclusions are drawn in Section 6.

2 | THE PHYSICS OF SECONDARY ROTORS

2.1 | Basic principles of operation

The following section will consider a turbine consisting of a rigid VAWT primary rotor, with secondary HAWT rotors attached at the primary rotor blade tips. The VAWT primary rotor is allowed to rotate freely around the vertical axis, and there is no power taken off from the low-speed shaft. The primary rotor speed is controlled solely through the thrust acting on the secondary rotors, and the only source of electrical power is that captured by the secondary rotors. Assuming that the primary rotor has sufficient inertia such that the rotor speed does not change considerably over a single rotor revolution, the primary rotor is at equilibrium when

$$\underbrace{\left[\frac{1}{\omega_P}\frac{1}{2}\rho A_P C_{P_p} U_0^3\right]}_{\overline{Q_P}} = N R_P \underbrace{\left[\frac{1}{2}\rho A_S \overline{C_{T_s} U_l^2}\right]}_{\overline{T_s}}. \tag{1}$$

Here, the subscripts $_P$ and $_S$ represent primary and secondary rotor variables respectively and the over-line $\overline{(\cdot)}$ represents variables averaged over a primary rotor revolution. ω represents the rotor rotational speed, ρ represents the air density, A represents the rotor area, C_P and C_T represent the rotor power and thrust coefficient, U_0 represents the free wind speed, U_I represents the inflow wind speed to the secondary rotors and N represents the number of secondary rotors and R represents the rotor radius. The rotor torque, Q, and thrust, T, are identified by the underbraces. The rotor coefficients are functions on the tip speed ratio, $\lambda_{[P/S]} = \omega_{[P/S]} R_{[P/S]} / U_{[0/I]}$. Dynamic simulations of the X-Rotor turbine[25] have shown that primary rotor speed fluctuations with an amplitude of 4.5% are present at rated wind speed, which indicates that the large inertia assumption is reasonable.

The control of the primary rotor speed can be achieved through controlling $\overline{T_S}$. Assuming the secondary rotors operate at a constant tip speed ratio, Equation (1) can be rearranged (noting) to define the thrust coefficient required to hold the primary rotor at an equilibrium operating point, essentially applying optimal torque control, giving

$$C'_{T_S}(\lambda'_S) = \frac{A_P}{NA_s} \frac{C'_{P_P}(\lambda'_P)}{\lambda'_P} \frac{U_0^2}{\overline{U_I^2}} \approx \frac{A_P}{NA_s} \frac{C'_{P_P}(\lambda'_P)}{\left(\lambda'^3_P + \frac{1}{2}\lambda'_P\right)}. \tag{2}$$

Here, dashed terms $(\cdot)'$ represent design values. The approximate equality in Equation (2) is obtained by approximating the U_I as the sum of the free wind speed and the apparent wind speed due to the rotation of the primary rotor:

$$U_I = U_0 cos(\theta) + \omega_P R_P, \tag{3}$$

where θ defines the angle of the azimuth of the VAWT primary rotor blade. This assumption is discussed in Section 2.4.

The efficiency of power conversion between the primary and secondary rotors (defined as the proportion of the primary rotor aerodynamic power that is captured by the secondary rotors), η, is given by the ratio of the energy captured by the secondary rotors over one primary rotor revolution against the work done by the thrust on the secondary rotors over a revolution. Whilst operating at a constant secondary rotor tip speed ratio, this yields

$$\eta = \frac{N\overline{P_s}}{\overline{P_P}} = \frac{N\overline{P_s}}{\omega_P N R_P \overline{T_s}} \approx \frac{C_{P_S}}{C_{T_S}} \left(\frac{1 + \frac{3}{2}\lambda_P^{-2}}{1 + \frac{1}{2}\lambda_P^{-2}}\right). \tag{4}$$

Here, the approximate equality is again obtained through Equation (3). The relationships given in Equations (2) and (4) are key to understanding the intrinsically coupled behaviour of the primary and secondary rotors. From Equation (4), it is clear that the efficiency is primarily driven by the ratio C_{P_S}/C_{T_S}. However, the design thrust coefficient of the secondary rotor is dictated by the primary rotor configuration, as in Equation (2).

Generally, the maximum attainable value for the ratio C_{P_S}/C_{T_S} is achieved by lowering the design thrust coefficient. This can be understood through an actuator disk representation of the secondary rotors, where the fraction C_{P_S}/C_{T_S} is equal to $(1-a)$, with a representing the axial induction factor. From this relationship, it is clear that the design induction factor (and therefore thrust coefficient) should be minimized in order to maximize the conversion efficiency. C'_{T_S} can be reduced by increasing the ratio of the total swept area of the secondary rotors to the primary rotor area, increasing the primary rotor tip speed ratio or decreasing the primary rotor power coefficient. As the total aerodynamic efficiency of the rotor is also dictated by the primary rotor power coefficient, it is clear that latter option is not desirable. The absolute limitations and design compromises associated with secondary rotor swept area and the primary rotor tip speed ratio are discussed in Section 2.2. A more complete description of the secondary rotors is proposed in 2.3, which leads to a more nuanced understanding of the optimum secondary rotor design.

2.2 | Limitations on secondary rotor design

In order to effectively understand the design of secondary rotors, the limitations of the rotor design must considered. There are two key design limitations on the secondary rotors:

1. The apparent tip speed of the secondary rotor is limited to a value U_{max} in order to avoid the effects of aerodynamic compressibility and excessive aero-acoustic emissions.

$$\omega_S R_S \leq U_{Max}.$$

Compressible computational fluid dynamic simulations and further experimental and operational knowledge are required to understand the exact limiting value (U_{Max}). In this study, a value of 184 m/s (as proposed in Leithead et al[4]) is considered as a baseline, and the effects of maximum tip speed are discussed in Section 4.

2. To avoid compromising conversion efficiency in the power electronics, the rotational speed of the secondary rotors must satisfy

$$\omega_S = \frac{2\pi f_r}{p},$$

at rated power, where f_r represents the nominal electrical frequency of the secondary rotor generator and p represents the number of pole pairs.

Limitation 1 provides a strict limit on the product of the primary and secondary rotor tip speed ratio and rated wind speed, U_R:

$$\lambda'_P \lambda'_S U_R \leq U_{Max}. \tag{5}$$

Additionally, when combined with limitation 2, a maximum limit on the secondary rotor radius is provided:

$$R_S \leq \frac{pU_{Max}}{2\pi f_r}. \tag{6}$$

For all reasonable rotor configurations, η is maximized by taking Equation (5) in the upper limit so as to maximize the secondary rotor tip speed ratio thus maximizing the achievable C'_{P_S} for a given C'_{T_S}. Similarly, η is maximized by taking the upper limit of Equation (6) through maximizing the secondary rotor area, decreasing C'_{T_S}.

2.3 | Secondary rotor representation

Representing the secondary rotors as optimally designed allows the rotors to be described in a closed-form solution once the required axial induction has been calculated. This allows for an accurate representation of the optimal secondary rotor behaviour, including the effects of tip/hub loss, tangential induction, drag losses and the turbulent wake effect. The optimally designed BEM approach is preferred in this study as it allows for a transparent and computationally efficient means of finding the maximum achievable secondary rotor performance.

2.3.1 | Representation of the rotor hub

Prior to describing any representations of the secondary rotor, a key consideration is how to represent the large hub diameter expected in a secondary rotor system. For example, the X-Rotor secondary rotor design has a hub radius that is 17% of the rotor radius.[26] To calculate the aerodynamic coefficients of the rotor, only the contributions outside of the rotor hub are considered. The rotor thrust coefficient can then be calculated as the sum of the rotor thrust coefficient and the rotor hub thrust coefficient:

$$C_{T_S} = C_{T_A} + C_{T_h} x_h^2, \tag{7}$$

where C_{T_A} represents the aerodynamic thrust coefficient of the rotor, C_{T_h} represents the hub thrust coefficient and x_h represents the non-dimensional hub radius (R_h/R_S). The power coefficient remains unchanged. This method does not account for flow re-direction around the rotor hub.

2.3.2 | Optimized BEM representation

Previously, optimal BEM theory has focused on the design of rotors operating at the Betz limit[18]; however, this work extends the optimal BEM representation of a rotor to a rotor operating at an arbitrary thrust coefficient. The process presented here represents an extension of that provided in Jamieson[18] to include both tip and root losses and to be valid for high blockage cases. Whilst the high blockage cases $(a > 0.4)$ by their nature represent inefficient solutions, the solutions are included for completeness.

For a rotor with constant axial induction, the rotor thrust coefficient is given by

$$C_{T_A} = \begin{cases} 8a(1-a)\int_{x_h}^{1} F x dx & (a \leq 0.4) \\ 2\int_{x_{hub}}^{1} \left\{ \frac{8}{9} + \left[4F - \frac{40}{9} \right] a + \left[\frac{50}{9} - 4F \right] a^2 \right\} x dx & (a > 0.4) \end{cases}. \tag{8}$$

with the $a > 0.4$ case representing the integrated form of Buhl's tip correction for high blockage cases.[27] $F(x,a)$ represents the end loss coefficient and x represents the non-dimensional radial coordinate. The end loss coefficient is given by the production of the tip and root loss coefficients

$$F(x,a) = F_t F_r \tag{9}$$

with

$$F_t = \frac{2}{\pi} acos\left(exp\left\{ -\frac{B}{2}\frac{(1-x)}{x}\sqrt{1+\left[\frac{\lambda_S x}{(1-a)}\right]^2} \right\} \right) \tag{10}$$

$$F_r = \frac{2}{\pi} acos\left(exp\left\{ -\frac{B}{2}\frac{(x-x_{hub})}{x_{hub}}\sqrt{1+\left[\frac{\lambda_S x}{(1-a)}\right]^2} \right\} \right), \tag{11}$$

where B represents the number of blades on the secondary rotor. For simplicity, this tip loss formulation neglects the effect of tangential induction, following the example of Jamieson.[18] Whilst tangential induction becomes large toward the blade root, the effect of this assumption on rotor averaged power and thrust coefficients is shown to be small further in this section. From a given thrust coefficient, the axial induction factor can be back-calculated with

$$a = \frac{1}{2}\left(1 - \sqrt{1 - \frac{C_{T_A}/(1-x_{hub}^2)}{\int_{x_{hub}}^1 2Fxdx}} \right) \tag{12}$$

for $\left(C_{T_A} \le 1.92\int_{x_h}^1 F(x)xdx\right)$ and

$$a = \frac{36\int_{x_{hub}}^1 Fxdx - 20(1-x_{hub}^2) - 3\sqrt{24\int_{x_{hub}}^1 Fxdx\left[6\int_{x_{hub}}^1 Fxdx - 4(1-x_{hub}^2)\right] + C_{T_A}\left[50(1-x_{hub}^2) - 72\int_{x_{hub}}^1 Fxdx\right]}}{72\int_{x_{hub}}^1 Fxdx - 50(1-x_{hub}^2)} \tag{13}$$

for $\left(C_{T_A} > 1.92\int_{x_h}^1 F(x)xdx\right)$, where Equation (13) represents Buhl's modification of Glauert's correction for high induction factors[27] integrated along the blade length.

As the end loss coefficient is dependent on the induction factor, an iterative scheme is required to calculate the axial induction factor for a given thrust coefficient. This can be readily completed by initializing the end loss factor as 1 (i.e. no end losses), back-calculating the induction using Equations (12) and (13), updating the end loss estimate using the newly calculated axial induction factor and re-calculating the thrust coefficient. This process can be repeated using an updated end loss factor until the desired thrust coefficient is reached. Once the axial induction factor is obtained, the tangential induction factor can be calculated with

$$a_t(x) = \frac{\sqrt{\lambda_S^2 k^2 x^2 + 2\lambda kx - 4ak[\lambda_S x - k(1-a)] + 1} - (\lambda_S kx + 1)}{2\lambda_S kx} \tag{14}$$

where k represents the design lift-to-drag ratio of the aerofoil section for the secondary rotor. If a number of aerofoil sections are used, k can be readily updated from a scalar value to a lift-to-drag distribution; however, in this work, the secondary rotor is considered to consist of a single aerofoil section. The design value lift-to-drag ratio of the aerofoil section can be used over the full rotor span as it is assumed a-priori that the rotor twist distribution will be optimally designed in order for the blade to operate at its design angle of attack. The corresponding rotor power coefficient is given by

$$C_{PA} = \int_{x_h}^1 \frac{8a(1-a)F[k(1-a) - \lambda_S x(1+a_t)]\lambda_S x^2}{[\lambda_S kx(1+a_t) + (1-a)]}dx \tag{15}$$

for $(a \le 0.4)$ and

$$C_{PA} = \int_{x_h}^1 \frac{2\left[\frac{8}{9} + \left(4F - \frac{40}{9}\right)a + \left(\frac{50}{9} - 4F\right)a^2\right][k(1-a) - \lambda_S x(1+a_t)]\lambda_S x^2}{[\lambda_S kx(1+a_t) + (1-a)]}dx \tag{16}$$

for $(a > 0.4)$. This method facilitates the calculation of an optimal power coefficient for a rotor at an arbitrary design tip speed ratio and design thrust coefficient.

The corresponding chord distribution is given by

$$c(x) = \frac{8\pi a(1-a)F}{B\lambda(1+a_t)\sqrt{(1-a)^2+\lambda^2x^2(1+a_t)^2}\left[1+\frac{(1-a)}{k\lambda x(1+a_t)}\right]}\frac{R_s}{C_L'} \tag{17}$$

for $(a \le 0.4)$ and

$$c(x) = \frac{2\pi\left[\frac{8}{9}+\left(4F-\frac{40}{9}\right)a+\left(\frac{50}{9}-4F\right)a^2\right]}{B\lambda(1+a_t)\sqrt{(1-a)^2+\lambda^2x^2(1+a_t)^2}\left[1+\frac{(1-a)}{k\lambda x(1+a_t)}\right]}\frac{R_s}{C_L'} \tag{18}$$

for $(a > 0.4)$. With a twist given by

$$\beta(x) = atan\left[\frac{(1-a)}{\lambda_S x(1+a_t)}\right] - \alpha_0, \tag{19}$$

where α_0 represents the design angle of attack for the secondary rotor aerofoil section and $C_{L'}$ represents the design lift coefficient.

The thrust and power coefficients predicted by the optimal BEM formulation can be compared to the rotors described by the chord and twist distributions in Equations (17), (18) and (19) simulated in the BEM code Aerodyn[28]; the results are shown in Figure 2. In general, there is strong agreement in the achieved thrust coefficient over the full range of design thrust coefficients with a maximum error of 0.03 at a low tip speed ratio—high thrust coefficient design. The predicted power coefficient again shows strong agreement, with a maximum error of 0.02. As the efficient operation of the secondary rotors relies on a low thrust coefficient design, the zone in which the strongest agreement is present, the proposed analytical on-design representation of optimized rotors is considered valid for use in this study.

2.4 | Aerodynamic environment of the secondary rotors

Thus far, the inflow conditions of the secondary rotor have been assumed to be characterized by Equation (3); implicit in this characterization is the assumption that the velocity field induced by the primary rotor does not significantly affect the inflow of the secondary rotor. Primary rotor

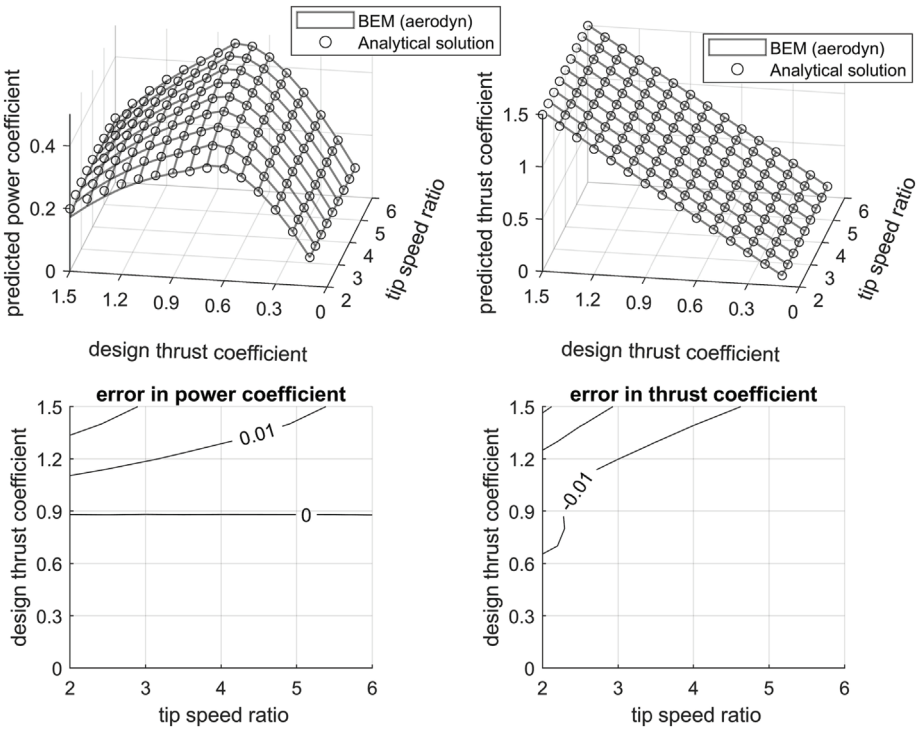

FIGURE 2 Validation of optimal designed blade element momentum (BEM) theory against BEM simulations for on-design rotor performance.

simulations using LLFVW models allow the velocity field around the primary rotor to be evaluated, facilitating the validation of this assumption through the evaluation of the velocity field at the attachment position of the secondary rotors.

An exemplar primary rotor from the X-Rotor project (rotor definition can be found in Leithead et al[4]) was simulated in the open-source LLFVW solver QBlade.[29] The rotor was simulated for 12 full rotations until the rotor thrust was fully converged. The flow field at the secondary rotor was then evaluated at 5-degree intervals over the full rotor sweep. The secondary rotors are attached such that the secondary rotor blade tip is 4.7 m below the primary rotor blade tip. The velocity normal to the secondary rotor plane is then averaged over the secondary rotor area and compared to the approximation in Equation (3), as shown in Figure 3. There is good agreement between the evaluated velocity field from the LLFVW simulations.

With the simplistic representation of the inflow velocity verified, there are still a number of uncertainties associated with the unique aerodynamic environment in which the secondary tip rotors operate. The orbital motion of the secondary rotors produces a curved wake. This curved wake may have implications for the tip loss formulations for the secondary rotor and is not consistent with the wake assumptions inherent in BEM theory. Additionally, the orbital motion induces a horizontal shear on the secondary rotor, and the combination of the rotational velocity and the mean flow also means that the secondary rotor is operating with an oscillating yaw offset. Whilst they are not considered in the optimal BEM representation of the rotor described in Section 2.3, these effects are intrinsically modelled by LLFVW codes; thus, a comparison between the simulated behaviour of the secondary rotor in orbital motion using the LLFVW method and the behaviour of the secondary rotor characterized by the inflow velocity given in Equation (3) and the power and thrust coefficients calculated in Equations (15), (16) and (8) allows for the approach provided in Section 2.3 to be validated.

The motion of the simulated secondary rotor was prescribed such that it followed a circular orbit was a radius of 75 m and a rotational speed of 0.76 rad/s, and the free windspeed was equal to 12 m/s. This is equivalent to the 5 MW exemplar X-Rotor design presented in Leithead et al[4] with a tip speed ratio of 4.75. The yaw angle of the secondary was scheduled such that the rotor normally aligned with the tangent to the circular motion, and the rotational speed of the secondary rotor was scheduled such that it would operate at an optimal tip speed ratio given the inflow assumption in Equation (3). Maximum power point tracking for the secondary rotors does not require a variable pitch strategy, and optimal speed control, through typical torque control, has been shown to be effective in dynamic simulations of the X-Rotor concept.[25]

The results in terms of rotor power production and axial thrust loading are shown in Figure 4. In the upwind rotor half, between 0 and π, the optimized BEM representation provides an excellent characterization of both power production and thrust loading on the rotor compared to the LLFVW simulations. In the downwind rotor half, however, the rotor encounters its own wake which leads to significant fluctuations in the power capture and thrust loading. This self-wake interaction is not modelled by the optimized BEM representation. It should be noted that the

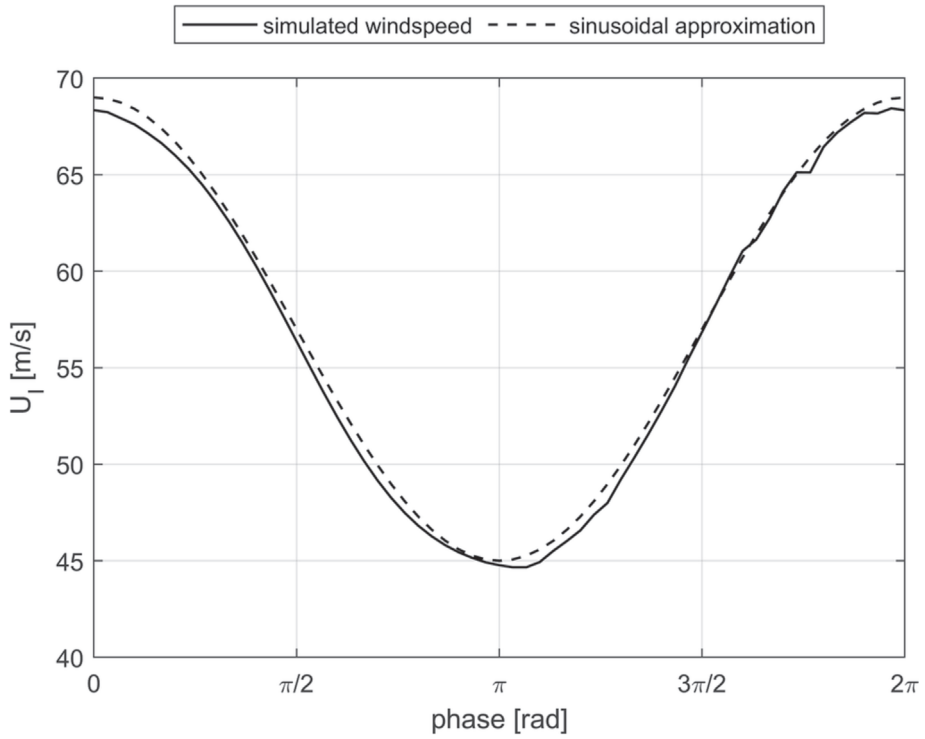

FIGURE 3 Verification of the assumption of an undisturbed inflow speed to the secondary rotors through the evaluation of the wind field normal to the secondary rotor plane from LLFVW simulations of the primary rotor.

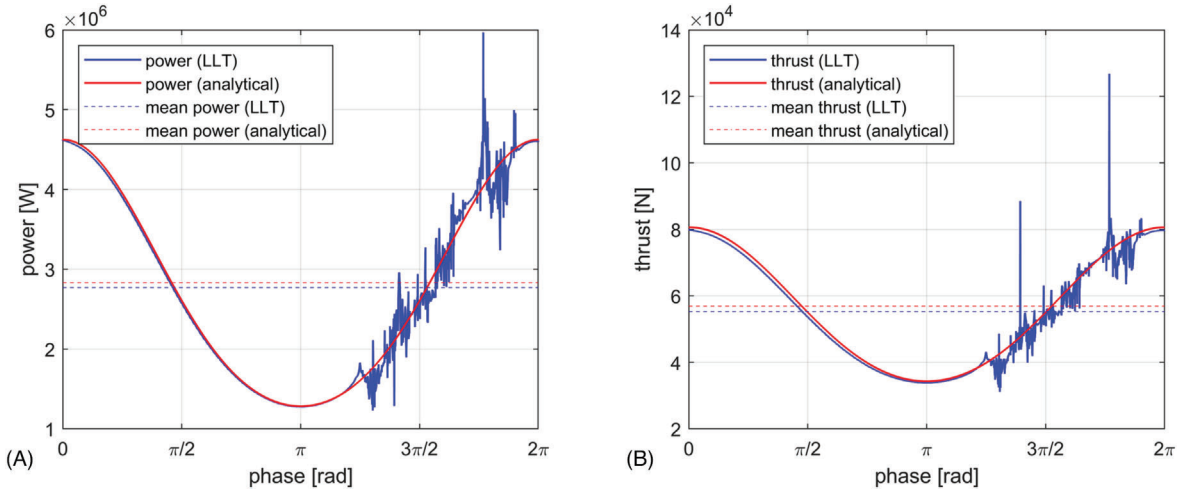

FIGURE 4 Comparison of an optimized BEM representation of a secondary rotor and an LLFVW representation, the blue trace labelled LLT represents the LLFVW results.

secondary rotor wake will be subject to strong interactions from the vortex system of the primary rotor wake, thus a fully coupled aerodynamic simulation is required to fully characterize the secondary rotor behaviour in the downwind rotor half. Additionally, the LLFVW model does not include viscous forces which drive the dissipation of the rotor wake. This implies that a higher fidelity computational fluid dynamics–based approach, which is required to fully understand the secondary rotor behaviour in the downwind rotor sweep.

Nonetheless, in terms of rotation-averaged behaviour, the models show good agreement, with the optimized BEM representation providing a rotation-averaged power production estimate 2.2% higher than the LLFVW model, and a rotation average thrust estimate 3.1% higher than the LLFVW model.

3 | A FRAMEWORK FOR PARAMETRIC ANALYSIS OF TURBINES UTILISING SECONDARY ROTORS

The design space of a turbine utilising secondary rotors for power take is high-dimensional, including variables associated with the primary rotor $(C_P,\ \lambda_P,\ A_P,\ U_R,\ N_S)$, the secondary rotor $(k,\ B)$, the drivetrain $(f_r,\ p,\ R_h,\ C_{T_h})$ and environmental variables (ρ, U_{Max}). In order to understand this design space and highlight both the region in which optimal solutions exist and the technological areas in which innovation can best be applied to increase energy capture, a parametric model of a turbine utilising secondary rotors is here developed.

For a given primary rotor configuration $\left(C'_{P_P},\lambda'_P,A_P,N_S\right)$ designed for a given rated wind speed (U_R), with a known tip speed limit (U_{max}) and defined drivetrain configuration (f_r,p) and a known rotor hub (r_h,C_{T_h}). The maximum realizable performance for a secondary rotor with a given lift-to-drag ratio, k, and number of blades, B, can be calculated using the design thrust coefficient defined in Equation (2), with the rotor area given by the upper limit of Equation (6), the design tip speed ratio given by the upper limit of Equation (5) and then employing method described in Section 2.3.

In order to accurately predict the aerodynamic efficiency of the secondary rotors, the rotor hub radius must also be well characterized. Assuming that the rotor hub scales linearly with the generator stator radius, similarity scaling dictates that the secondary rotor hub radius scales with the cube root of the rated torque of the secondary rotors. An initial design of an appropriate generator for the 5 MW X-Rotor turbine has been completed in Campos-Gaona et al,[26] which provides a design point to scale from.

As the rated torque on the generator can only be calculated once the aerodynamics of the secondary rotor have been characterized, an iterative loop must be included whereby the rotor hub is initialized at some representative value, and the secondary rotor design process completed to obtain an estimate of the rated torque on the secondary rotor. This rated torque is then used to calculate an updated rotor hub estimate and the process is repeated until the rotor design converges.

4 | RESULTS

This methodology can be applied to a baseline rotor configuration, with variables shown in Table 1. These variables are based on the baseline X-Rotor design presented in Leithead et al[4] alongside an updated estimate of the achievable power coefficient from Morgan and Leithead,[24] the drivetrain described in Campos-Gaona et al[26] and a representative estimate of the hub thrust coefficient.

TABLE 1 The baseline variables used for the parametric study, closely based on the variables used in the feasibility study.[4]

N_s	C_{P_p}	U_R (m/s)	U_{max}(m/s)	f_r (Hz)	p	R_{h0} (m)	Q_0 (kNm)	C_{T_h}	k	B
2	0.45	12	184	25	4	0.8	64.1	0.4	100	5

Note: R_{h0} and Q_0 represent the secondary rotor hub radius and design torque from which the hub radius can be scaled.

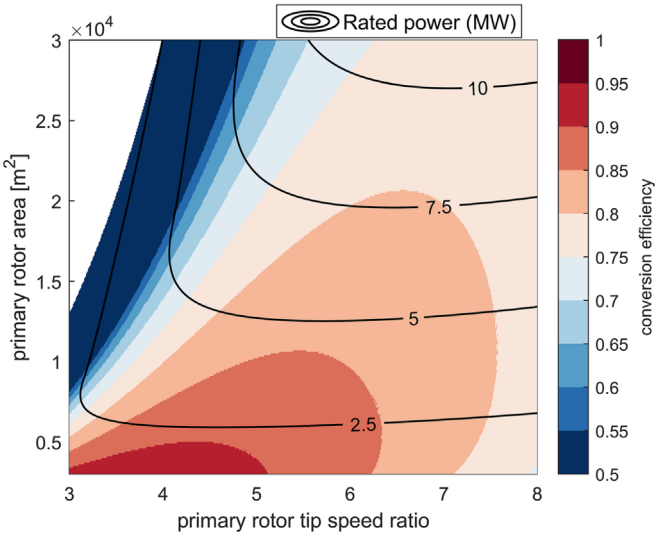

FIGURE 5 Efficiency contours for power conversion between the primary and secondary rotors, alongside rated power contours.

Using the baseline design variables in Table 1, and treating both the primary rotor area and the tip speed ratio as free variables, a banded colour map showing the conversion efficiencies achievable with optimally designed secondary rotors is plotted in Figure 5. The maximum tip speed ratio considered in this study is 8, corresponding to a primary rotor tip speed of 96 m/s, and a secondary rotor tip speed ratio of 1.91. Both the very high primary rotor tip speed ratio and the very low secondary rotor tip speed ratio make this upper bound an unlikely design choice; however, the range of solutions is shown for completeness. Alongside the banded colour map are solid black contours showing the rated power of a given rotor configuration. The locations of maximum conversion efficiency for a desired rated power can be easily located as the point on a given rated power contour corresponding to the lowest primary rotor swept area. This approach can be used as a guide to the optimal tip speed ratio that a primary rotor should be designed for, given a set of design variables and a desired rated power.

From Figure 5, it is clear that, with a fixed number of secondary rotors, the conversion efficiency decreases with increasing rated power. This occurs as an increase in primary rotor power requires increased thrust from the secondary rotors. As the secondary rotor area is fixed by the minimum rotational speed and maximum tip speed requirements, the secondary rotors must operate at higher thrust coefficients, decreasing the conversion efficiency.

Efficiency can be preserved during upscaling through the use of additional secondary rotors, increasing the total area swept by the secondary rotors and decreasing the design thrust coefficient. This is demonstrated in Figure 6, where the baseline turbine is augmented by including more secondary rotors, representing a two- and three-bladed design with either one or two secondary rotors per blade. The maximum achievable conversion efficiency is shown as a function of the rated power of the turbine for each of the four design configurations.

A conservative estimate of the nacelle mass can be generated by assuming that the total mass of the nacelle is equal to twice the mass of the generator

$$m_X = 2m_G, \tag{20}$$

where the generator mass is again generated through similarity scaling from the design detailed in Campos-Gaona et al.[26] As the secondary rotors are operating at a fixed rotational speed and the generator mass scales with rated torque, the combined nacelle mass estimate for a given power rating is independent of the number of secondary rotors employed. The nacelle mass can be treated as a proxy for the nacelle cost and is therefore considered an interesting variable for comparison. A full LCOE analysis for the baseline X-Rotor turbine is underway as part of the X-Rotor project[21]; however, LCOE estimation for novel wind turbine concepts is a complex task and outside of the scope of this paper. The nacelle mass estimate is shown in Figure 6 alongside reference HAWT drivetrain masses, obtained from the 5 MW NREL reference turbine,[30] the 10 MW DTU reference turbine[31] and the 15 MW IEA reference turbine.[32]

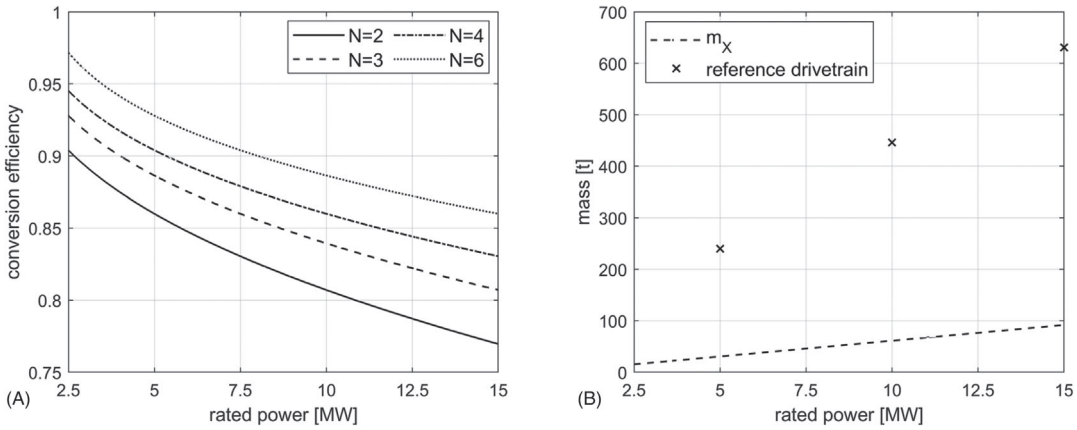

FIGURE 6 (A) Maximum achievable conversion efficiency between the primary and secondary rotor with practical design constraints on the secondary rotor. (B) Estimated generator mass compared to 5 MW, 10 MW and 15 MW reference turbine designs.

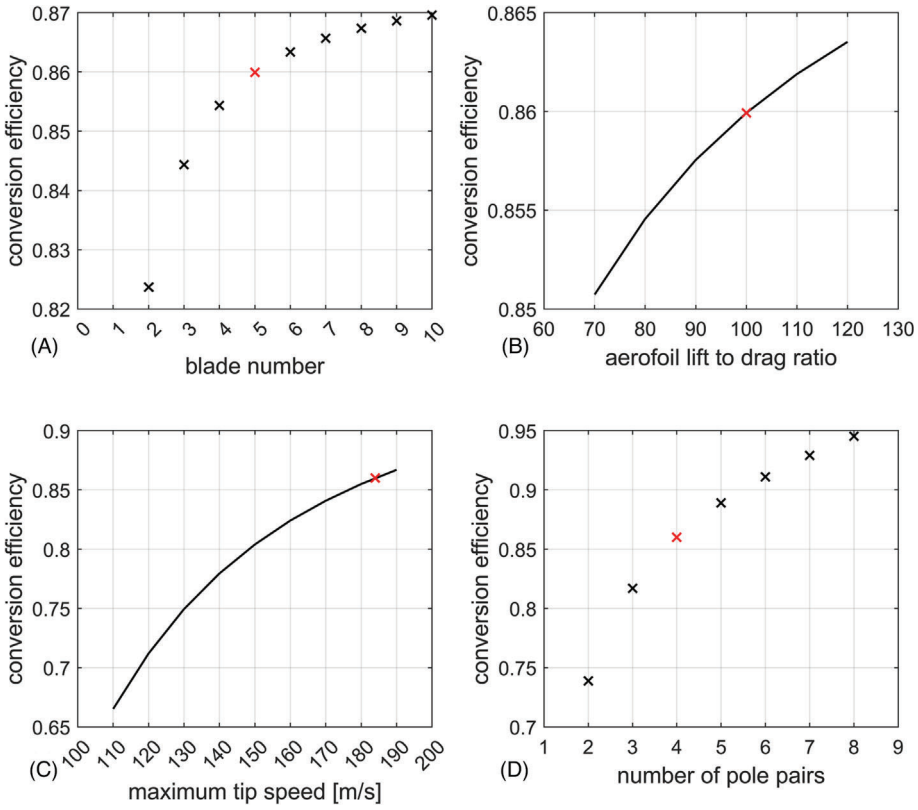

FIGURE 7 Effect of rotor and generator design parameters on aerodynamic conversion efficiency between the primary and secondary rotor.

Figure 7 shows the changes in conversion efficiency between the primary and secondary rotor as a function of the number of blades used on the secondary rotors (a), the aerofoil lift-to-drag ratio (b), the maximum tip speed limit (c) and the number generator pole pairs (d). Other than the independent variables labelled explicitly on the *x*-axis, all other turbine variables are given in Table 1.

5 | DISCUSSION

The efficiency contours in Figure 5 can be understood through Equations (2) and (4). As the secondary rotor area is fixed by the constraints in Section 2.2, and the primary rotor power coefficient is considered fixed, the required thrust coefficient varies linearly with increased primary rotor

area and approximately inversely to the cube of the design tip speed ratio $\left(\lambda'^{3}_{P}+\lambda'_{P}\right)^{-1}$. The secondary rotor design tip speed ratio is inversely proportional to the primary rotor tip speed ratio.

For a given primary rotor–rated power, the maximum realizable efficiency of power conversion increases with increasing primary rotor tip speed ratio due to the increasing power-to-thrust ratio for the secondary rotor as the design axial induction for the rotor decreases. As the primary rotor tip speed ratio increases further, the efficiency of energy conversion decreases for two reasons: Firstly, the performance of the secondary rotors is decreased at the secondary rotor tip speed ratio decreases, as in Equation (5). Secondly, at very low design axial induction factors, the parasitic thrust from the secondary rotor hub provides a larger contribution to the total thrust secondary rotor thrust and significantly decreases performance.

Figure 6, can again be readily understood with Equations (2) and (4). As the secondary rotor swept area is fixed by the drivetrain and tip speed constraints, the design thrust coefficient is inversely proportional to the number of secondary rotors utilized. The efficiency is increased as the power-to-thrust coefficient ratio decreases. The overall performance gains from the inclusion of more secondary rotors are clear; however, the excess parasitic drag from the support structure and the additional mechanical complexity must be considered in the design task. It is clear, however, that efficiency can be maintained during up-scaling by increasing the number of secondary rotors utilized. Utilizing a 2.5 MW rated secondary rotor, as in Leithead et al,[4] the maximum achievable conversion efficiency is shown to be 87%; however, through utilizing a 1.25 MW rated secondary rotor (thus doubling the number of rotors employed), the maximum achievable efficiency increases to 90%. Whilst direct upscaling of the secondary rotors is a possible means of increasing the rated power without sacrificing conversion efficiency, an increase in the secondary rotor radius will necessitate a decrease in the secondary rotor speed and consequently increase the torque in the secondary rotor drivetrain. This process repeats the problematic 'square-cube' scaling inherent in upscaling traditional wind turbine drivetrains, albeit from a more advantageous starting point. Through the inclusion of additional secondary rotors, the drivetrain costs scale linearly with the power rating in a manner analogous to multi-rotor systems. Because of this, upscaling through the inclusion of additional secondary rotor systems is currently seen as the most preferable option.

Figure 6B clearly shows the potential for drivetrain mass reduction facilitated by the use of secondary rotors, with the secondary rotor nacelle mass reduced by 87%–85%, under a conservative estimate compared to reference HAWT drivetrains. It is interesting to note that the reference turbine nacelle masses scale approximately linearly with rated power, rather than with an exponent of 3/2 as would be expected; this can be understood to be driven by innovations in drivetrain design, with the configuration shifting from a high-speed gearbox in the 5 MW design to a medium-speed gearbox in the 10 MW design and a direct drive drivetrain in the 15 MW design.

Figure 7 shows the effect of various design features and constraints on the maximum realizable conversion efficiency for the baseline X-Rotor design described in Table 1. As tip losses effect both the thrust and power coefficient equally, the effect of increasing blade number on the conversion efficiency cannot be explained by stating that the lower tip losses lead to high conversion efficiencies. It must instead be understood that by limiting tip losses, the rotor can operate at a lower design induction, thus moving the operating point to a location with a higher power-to-thrust coefficient ratio. As the secondary rotors are representative of only a small portion of the cost of the X-Rotor system, the increased engineering complexity and cost associated with a larger number of blades becomes a smaller factor in terms of cost, allowing for a five-bladed secondary rotor design, which significantly increases the power captured without imparting unmanageable bending stresses in the blade. The effect of the secondary rotor design lift-to-drag ratio on the conversion efficiency is considerably smaller. This may allow for thicker aerofoils to be used, which can lower the bending stresses in the secondary rotor blades.

The maximum allowable tip speed directly impacts the maximum allowable swept area of the secondary rotor through Equation (6), the effect on the conversion efficiency can be understood through Equations (2) and (4). The decrease in the secondary rotor swept area increases the design thrust coefficient for the secondary rotor thus decreasing the power to thrust coefficient ratio. This effect is very significant in terms of conversion efficiency, and the characterization of the maximum allowable tip speed for secondary rotors has not yet been completed. It is therefore of the utmost importance to properly understand the physical constraints on the tip speeds for the secondary rotors to facilitate efficient design.

The effect of increasing the number of pole pairs in the generator can be seen to have the opposite effect, introduced through the same relationship (Equation 6). Increasing the number of pole pairs facilitates an increased rotor area allowing the secondary rotors to operate at lower design thrust coefficients and increasing the power to thrust coefficient ratio. It should be noted that excessive expansion of the secondary rotor radius is not advised as, through increasing the size of the secondary rotors, their rotational speed must decrease to maintain tip speed limits and the drivetrain torque must increase, decreasing the generator mass savings achieved through the use of secondary rotors.

An important aspect of the design of offshore wind turbines is the control of energy injection during a grid fault (or loss of connection) and the ability to enact an emergency stop. In modern HAWTs, this can be completed through pitch control enacted with the use of back-up batteries with a parking brake to lock the rotor.[33] However, many VAWTs are not pitch controlled and a number of mechanisms have been proposed for emergency stops including mechanical brakes, aerodynamic spoilers and hydrodynamic brakes.[34] In the case of the X-Rotor, the upper blades are pitch controlled and will facilitate emergency stop actions, whilst a mechanical brake (attached to the primary rotor shaft) will facilitate the locking of the rotor, much like a traditional HAWT. As the secondary rotors are designed for a low tip speed ratio and therefore have an aggressive twist distribution, their thrust coefficient does not necessarily monotonically increase with tip speed ratio, and the turbine can begin to enter a propeller mode. This implies that over-speeding of the secondary rotors cannot be relied on as a means of braking the primary rotor, although the use of spoilers attached to the secondary rotor nacelle could be explored.

6 | CONCLUSION

This work has developed a parametric framework that can determine the aerodynamic efficiency of a vertical-axis wind turbine utilizing secondary rotors for power take-off. The approach is based on an extension of BEM-based optimal rotor design theory for arbitrary thrust loading, which facilities the representation of the on-design behaviour of an optimally designed rotor without the need for aerodynamic simulations. The design point for the secondary rotor is determined to optimally control the primary rotor speed under constraints imposed by drivetrain and tip speed limitations.

The BEM-based optimal design approach has been successfully validated against steady BEM simulations, and the simplified characterization of the inflow conditions for the secondary rotor has been verified using LLFVW simulations of an exemplar primary rotor. The BEM-based optimal design approach has been compared to LLFVW simulations representative of the complex aerodynamic environment of the secondary rotors. The mean power and thrust values were well reproduced (with 2.3% and 3.0% errors, respectively), although the fluctuations due to the rotor wake interaction are not accounted for. Coupled primary and secondary rotor simulations that model viscous effects are required to further verify secondary rotor performance in the downwind rotor sweep. The effect of the secondary rotor wake must also be considered on the aerodynamic performance of the primary rotor. The distance between the primary rotor blade tip and the secondary rotor will be a key variable in determining the strength of the interaction between the primary rotor tip vortex and the wake of the secondary rotor. Additionally, unsteady aerodynamic effects at the blade element scale were not accounted for, and simulations including dynamic stall models should be completed in order to perform detailed design work.

This framework was then used on an exemplar primary rotor configuration, demonstrating how the optimal primary rotor design is scale dependent, and how the efficiency of power conversion can be maintained at high rated powers through the inclusion of more secondary rotor units. With a secondary rotor unit rated at 2.5 MW, as in Leithead et al,[4] the maximum conversion efficiency between the primary and secondary rotors is found to be 87%. Whilst this is considerably lower than the efficiency of a HAWT drivetrain, it facilitates a nacelle mass reduction between 85% and 87%. The effect of secondary rotor design parameters on the maximum achievable conversion efficiency is investigated and it is found that utilizing a high blade number is encouraged to allow the rotor to operate at a lower design induction factor. The maximum tip speed strongly affects the maximum achievable conversion efficiency by limiting the allowable rotor size, and research is required to properly characterize the tip speed limits. It is encouraging that this effect can be mitigated by increasing the number of pole pairs utilized in the secondary rotor generator, facilitating a lower rotational speed and an expanded rotor. Excessive exploitation of this approach is not advised, however, as it reduces the benefits provided by the use of secondary rotors (low magnetic material usage, lightweight drivetrain).

This paper presents the results of exploratory research and has utilized a number of assumptions that require further investigation. Three key areas that require further consideration, which directly effect the work presented here, are as follows:

1. an investigation in the aerodynamic coupling between the primary and secondary rotor;
2. the determination of the maximum practicable tip speed for the secondary rotors;
3. an investigation into the parasitic drag associated with the structural members attaching the secondary rotor to the primary rotor tip.

The X-Rotor concept itself is at a low technology readiness level, and there is, of course, a considerable amount of work outside of the scope of this paper required to bring the concept towards commercial readiness. Much of this work is underway as part of the H2020 X-Rotor project.[20]

ACKNOWLEDGEMENTS

The authors would like to acknowledge their funding from the EU H2020 project XROTOR (Grant/Award Number: 101007135) and the EPSRC Centre for Doctoral Training in Wind and Marine Energy Systems (Grant/Award Number: EP/S023801/1).

CONFLICT OF INTEREST STATEMENT

N/A.

DATA AVAILABILITY STATEMENT

As the importance of this work is predominantly the development of a framework for optimal secondary rotor design, the data presented in figures are predominantly there to demonstrate the capability of the framework and provide general points of discussion. For that reason, the authors believe that the underlying data will not be of significant interest to the readers. If the reviewer believes that the data are important and therefore should be made available, the authors can provide the data that technical figures are generated from.

PEER REVIEW

The peer review history for this article is available at https://www.webofscience.com/api/gateway/wos/peer-review/10.1002/we.2901.

ORCID

Laurence Morgan https://orcid.org/0009-0000-9880-3589

James Carroll https://orcid.org/0000-0002-1510-1416

REFERENCES

1. IPCC. In: Pörtner HO, Roberts DC, Tignor M, et al., eds. *Impacts, Adaptation and Vulnerability. Contribution of Working Group II to the Sixth Assessment Report of the Intergovernmental Panel on Climate Change*. Cambridge University Press; 2022.
2. IRENA. *World Energy Transitions Outlook 2022: 1.5°C pathway*. International Renewable Energy Agency; 2022.
3. GWEC. In: Lee J, Zhao F, eds. *Global Wind Report 2021*. Global Wind Energy Council; 2021.
4. Leithead W, Camciuc A, Amiri AK, Carroll J. The X-Rotor offshore wind turbine concept. *J Phys: Conf Ser*. 2019;1356(1):012031. doi:10.1088/1742-6596/1356/1/012031
5. Nejad AR, Keller J, Guo Y, et al. Wind turbine drivetrains: state-of-the-art technologies and future development trends. *Wind Energy Sci*. 2022;7(1):387-411. doi:10.5194/wes-7-387-2022
6. Stehly T, Duffy P. *2020 cost of wind energy review*. NREL; 2020.
7. Carroll J, McDonald A, Dinwoodie I, McMillan D, Matthew R, Lazakis I. Availability, operation and maintenance costs of offshore wind turbines with different drive train configuration. *Wind Energy*. 2017;20(2):361-378. doi:10.1002/we.2011
8. Carroll J, Mcdonald A, Mcmillan D. Failure rate, repair time and unscheduled O&M cost analysis of offshore wind turbines. *Wind Energy*. 2016;19(6):1107-1119. doi:10.1002/we.1887
9. Jamieson P, Morgan L. *Trends, prospects and R&D directions in wind turbine technology*. Elsevier; 2022.
10. Pavel CC, Lacal-Arántegui R, Marmier A, et al. Substitution strategies for reducing the use of rare earths in wind turbines. *Resour Policy*. 2017;6(52):349-357. doi:10.1016/j.resourpol.2017.04.010
11. Alves Dias P, Carrara S, Plazzotta B. *The role of rare earth elements in wind energy and electric mobility*. Publication office of the European Union; 2020.
12. Li J, Peng K, Wang P, et al. Critical rare-earth elements mismatch global wind-power ambitions. *One Earth*. 2020;7(3):116-125. doi:10.1016/j.oneear.2020.06.009
13. Veers P, Sethuraman L, Keller J. Wind-power generator technology research aims to meet global-wind power ambitions. *Joule*. 2020;4(9):1861-1863. doi:10.1016/j.joule.2020.08.019
14. Sieros G, Chaviaropoulos P, Sørensen JD, Bulder BH, Jamieson P. Upscaling wind turbines: theoretical and practical aspects and their impact on the cost of energy. *Wind Energy*. 2012;1(15):3-17. doi:10.1002/we.527
15. Watson S, Moro A, Reis V, et al. Future emerging technologies in the wind power sector: a European perspective. *Renew Sustain Energy Rev*. 2019;113:109270. doi:10.1016/j.rser.2019.109270
16. Spenser JP. *Vertical challenge: the hiller aircraft story*. University of Washington Press; 1992.
17. de Vries O. Fluid Dynamic Aspects of Wind Energy Conversion. AGARD 1979 July;.
18. Jamieson P. *Innovation in wind turbine design*. 2nd ed. Wiley; 2018. doi:10.1002/9781119137924
19. Jamieson P. Top-level rotor optimisations based on actuator disc theory. *Wind Energy Sci*. 2020;5(2):807-818. doi:10.5194/wes-5-807-2020
20. X-Rotor cordis page. Accessed: 11/09/2022. https://cordis.europa.eu/project/id/101007135
21. X-Rotor website. Accessed: 11/09/2022. https://xrotor-project.eu/
22. McMorland J, Flannigan C, Carroll J, et al. A review of operations and maintenance modelling with considerations for novel wind turbine concepts. *Renew Sustain Energy Rev*. 2022;165:112581. doi:10.1016/j.rser.2022.112581
23. Flannigan C, Carroll J, Leithead W. Operations expenditure modelling of the X-Rotor offshore wind turbine concept. *J Phys: Conf Ser*. 2022;6(3):2265. doi:10.1088/1742-6596/2265/3/032054
24. Morgan L, Leithead W. Aerodynamic modelling of a novel vertical axis wind turbine concept. *J Phys: Conf Ser*. 2022;5(1):2257. doi:10.1088/1742-6596/2257/1/012001
25. Morgan L, Stock A, Leithead W. X-ROTOR WP3 D3.1 Control Simulation model for the X-Rotor Concept. 2021. doi: 10.5281/zenodo6967521
26. Campos-Gaona D, Stock A, Leithead W, Anaya-Lara O, Morgan L. X-ROTOR WP5 D5.1 Secondary rotors and power train design. 2021. doi: 10.5281/zenodo6973849
27. Buhl ML. A New Empirical Relationship between Thrust Coefficient and Induction Factor for the Turbulent Windmill State. Technical Report NREL/TP-500-36834. 2005.
28. Moriarty PJ, Hansen AC. AeroDyn Theory Manual. Technical Report NREL/TP-500-36881. 2005.
29. Marten D, Lennie M, Pechlivanoglou G, Nayeri CN, Paschereit CO. Implementation, optimization, and validation of a nonlinear lifting line-free vortex wake module within the wind turbine simulation code QBLADE. *J Eng Gas Turbine Power*. 2016;138(7):1-10. doi:10.1115/1.4031872
30. Jonkman J, Butterfield S, Musial W, Scott G. Definition of a 5-MW Reference Wind Turbine for Offshore System Development. Technical Report NREL/TP-500-38060. 2009.
31. Bak C, Zahle F, Bitsche R, et al., Description of the DTU 10 MW Reference Wind Turbine; 2013.
32. Gaertner E, Rinker J, Sethuraman L, Anderson B, Zahle F, Barter G. Definition of the IEA Wind 15-Megawatt Offshore Reference Wind Turbine. NREL. 2020. https://github.com/IEAWindTask37/IEA-15-240-RWT
33. Burton T, Jenkins N, Sharpe D, Bossanyi E. *Wind Energy Handbook*. John Wiley & Sons; 2011.
34. Wang K, Hansen MOL, Moan T. Dynamic analysis of a floating vertical axis wind turbine under emergency shutdown using hydrodynamic brake. *Energy Procedia*. 2014;53:56-69. doi:10.1016/j.egypro.2014.07.215

How to cite this article: Morgan L, Leithead W, Carroll J. On the use of secondary rotors for vertical axis wind turbine power take-off. *Wind Energy*. 2024;1-14. doi:10.1002/we.2901